Hindawi
Mathematical Problems in Engineering
Volume 2019, Article ID 2751815, 15 pages
https://doi.org/10.1155/2019/2751815

Research Article

Experimental and Numerical Analysis and Prediction of Ground Vibrations Due to Heavy Haul Railway Viaduct

Jingjing Hu,[1,2] **Yi Luo**,[1] **and Jiayun Xu**[1]

[1]*Hubei Key Laboratory of Roadway Bridge & Structure, Wuhan University of Technology, China*
[2]*School of Civil Engineering and Architecture, Wuhan University of Technology, China*

Correspondence should be addressed to Yi Luo; yluo@whut.edu.cn

Received 12 September 2018; Revised 29 November 2018; Accepted 9 January 2019; Published 13 February 2019

Academic Editor: Gisella Tomasini

The ground vibration wave induced by the viaduct section of the heavy freight wagons is transformed into the ground vibration problem under the condition of point source excitation after it is transmitted to soil through pier. When the speed and axle load of wagon become larger and larger, the impact on the surrounding buildings will also increase. In this paper, the ground vibration around Shenshan Village in section of Shuo-Huang railway line is monitored and numerical analyzed; the 3D numerical model of the Bridge-Pier-Field-House system is established. The relationship between peak vibration velocity (PPV) and the distance to the pier caused by heavy freight wagons at different speeds and different type of wagons is analyzed. The power function relationship between the two when measuring line perpendicular to the centerline of railway is verified. Based on the modified Sodev's equation, the relationship between PPV of ground points and wagon speed, axle load, and soil properties is proposed, and the value of every parameter in the formula is discussed in detail. The concept of energy index is put forward for the first time in the formula, and the relationship between energy index and wagon speed and wagon weight is analyzed by regression analysis. The accuracy of the calculation model and prediction formula is verified by comparing field test results; an analytical method is proposed to predict the ground vibration induced by viaduct.

1. Introduction

Railway is one of the most efficient transport systems in recent years; railway transportation develops very fast in China and abroad. With the development of transportation, the vibration caused by railways has an increasing impact on the environment. The environmental vibration caused by traffic load has the characteristics of repeatability and long-term. When it exceeds a certain level, it will affect the daily life and work of people in nearby buildings. When the vibration reaches a larger level, it may also cause damage to the structure of the building, thus affecting the normal function of the building [1–3].

On the other hand, due to the influence of terrain, more and more sections are designed as railway viaducts to ensure the smoothness of the line [4]. For example, the total length of the Seoul-Busan high-speed railway in Korea is 412km, the highest running speed is 300km/h, and the viaduct proportion is 27.1%. The Madrid-Seville high-speed railway in Spain has 31 viaducts with a total length of 15 km; the bridge ratio is 3.2%. The Beijing-Shanghai railway line has a total length of 1318 km, with 244 main bridges and a total length of 1060km. The bridge length accounts for 80.7% of the total line. However, the study of railway viaduct mostly focuses on the deformation and stability of bridges, which is quite complex due to the vehicle-coupled-guideway vibration [5–7]. Due to the different ways of excitation, the ground vibration caused by viaducts should also be concerned [8, 9].

On the other hand, with heavy load, long marshalling, and fast running speed, the dynamic effect of heavy freight wagons is stronger than that of ordinary trains, and the dynamic influence of wagons on the railway structure and its surrounding structures is more serious [10, 11]. The environmental vibration problem caused by the railway viaduct system involves many complicated dynamic systems such as wagons, bridges, piers, and sites and buildings, involving a large number of nonlinear problems [1, 12, 13]. Usually the system is decomposed into several subsystems to study

separately. The current theoretical research has not yet reached a high degree of precision or obtained a simplified analytical solution. Field measurements are the most common means of studying such problems [14–16].

However, railway line is usually long and the complexity of the problem is high, given the dynamic interaction between distinct domains, namely, the train, the viaduct, the ground, and the building. It is not realistic to detect each area nearby the line. As response to these needs, it is necessary to put forward the general law of ground vibration attenuation and to provide a method for evaluating the magnitude of train vibration in a viaduct area to be built.

Vibration assessment is a key element of the environmental impact assessment process for railway projects. For the propagation and attenuation law of ground vibration, many scholars have put forward different prediction formulas. They can be broadly classified into two categories: one is the amplitude representation and the other is the vibration level representation [17–19]. Among them, Bornitz [20] put forward the attenuation formula of ground vibration amplitude when disturbance force acts on the surface of half space of soil, considering the geometric attenuation of the vibration propagation and the medium absorption attenuation and the influence of propagation distance of the vibration. G. Volberg [21] based on tests at three different sites regressed the relationship between the vibration level and train speed. Chen Jianguo et al. [22] established an environmental vibration prediction formula based on the results of finite element vibration analysis. The formula reflects the logarithmic relationship between vibration acceleration level and distance and also considers the vibration level correction values of train speed, bridge span, and unit length and quality of the bridge by the additional function method. However, most of the above formulas can only reflect the attenuation relationship of vibration with distance or wagon speed and cannot clearly reflect the influence of geological conditions. More accurate prediction formulas should be put forward.

A large number of studies have shown that the vibration velocity and vibration frequency of the particle are closely related to the damage of the building [23–25]. It can directly reflect the vibration energy and play an important role in the evaluation of the vibration of building. Accurate prediction of the peak vibration velocity (PPV) of ground points under different site conditions is of great significance. In the field of traffic environment vibration, especially for the ground vibration caused by the heavy freight wagons, there are few studies using PPV as the evaluation index. Regarding the organization of the paper, firstly, a finite element model of track, box girder, pier, field, and building is established on the basis of field test. Numerical result of vibration response of ground and structure is studied by analyzing vibration velocity and spectra induced by trains of different weight and speed on a railway viaduct. Based on modified Sodev's formula, the relationship between PPV and wagon speed, wagon weight, distance, and site is established. Finally, regression analysis is used to discuss the procedures of determining each parameter in the forecast formula.

2. Field Test of Railway Viaduct in Shenshan Village

Shuo-Huang railway is an important part of the second largest channel of the "West-East Coal Transportation" in China. The total length of the railway is nearly 600 km, the transportation capacity exceeds 255 million tons, and the freight volume increases by tens of millions of tons every year. It is located in the connecting area between mountainous area and plain. The relative height difference is 200m-700m. The length of the bridge section accounts for more than 10% of the total length. In the northeast of Yuanping City, Shanxi Province, Shuo-Huang Heavy-Haul Line crosses Shenshan Village in the form of viaducts. The area is densely populated and there are a large number of residential buildings within 30 meters of the railway line, as shown in Figure 1.

Shuo-Huang railway is a first-class electrified railway with double track, ballast track, jointless track, and the rail of 60 kg/m. The commonly used types of trucks are C64k, C70, and C80. The axle weights of heavy freight wagons are about 21t, 23t, and 25t, and the axle weights of empty wagons are about 5.8t, 6.0t, and 5.0t. The unspring mass of the wagon is about 1500 kg per wheel set.

Monitoring points in the field test can be divided into 3 parts: pier measuring points, site measuring points, and house measuring points, as shown in Figure 2. Among them, the site measuring points are mainly arranged on two different routes perpendicular to the viaduct axis (Rout MR and Rout PL). Limited by the conditions of the site, there are four measuring points on each of the two lines, and the distance between adjacent points is not completely equal. Based on measured data, the basic law of site vibration attenuation on two measuring routs is put forward. In order to further analyze and verify the proposed rules, a numerical model is set up below.

3. Numerical Analysis of Ground Vibration Induced by Viaduct

A 3D numerical model is established to analyze the vibration attenuation rule of site points under various wagon speed and axle load more deeply. Due to the complexity of rail system, the tracks and the ballast were considered to be contact directly; the field was considered as homogeneous sand soil.

3.1. Calculation Model and Parameter Setting. According to the actual site conditions of Shenshan railway viaduct, a numerical model of Bridge-Pier-Field-House system is established using ANSYS/LS-DYNA, as can be seen in Figure 3, which shows the finite elements (FE) mesh of the cross section. The size of the field model is 125m length perpendicular to the tracks direction and 132.5m in the direction of the tracks, including 5 piers, with each span of 26.5m. The thickness of the soil layer is 8.0m, under which there is bed rock; the nodes at the bottom boundary are fixed in all directions to simulate the bedrock. Pier foundation adopts independent foundation. The maximum element size is 2.25 m; the minimum element size is 0.2m, satisfying the requirements of an element dimension in finite element analysis. The

Figure 1: The field site of Shenshan railway viaduct.

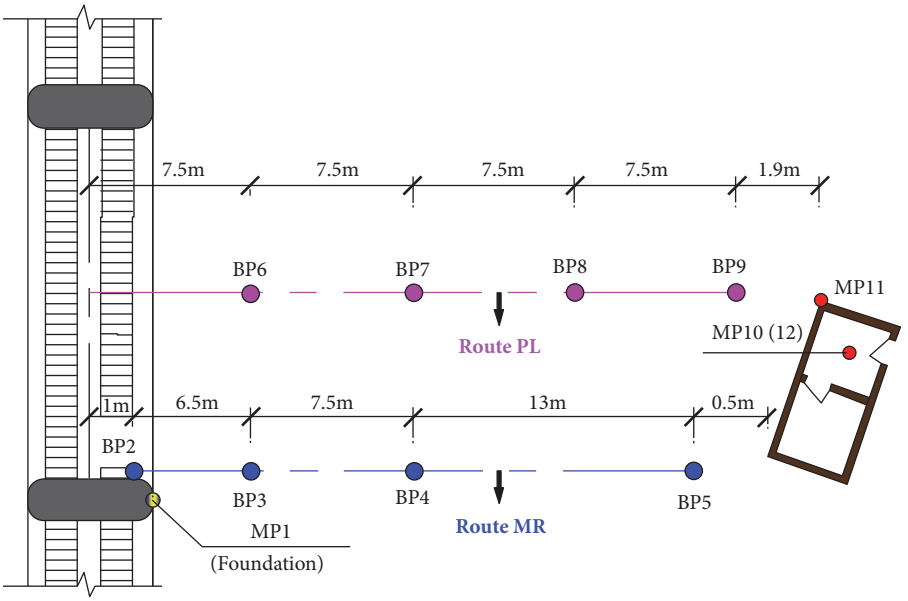

Figure 2: Layout of measuring points in the field test (unit: m).

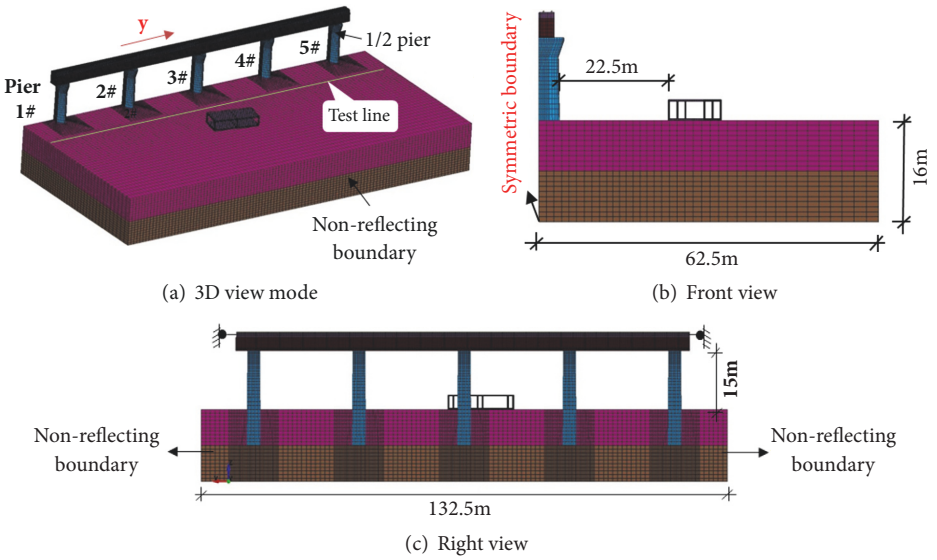

(a) 3D view mode

(b) Front view

(c) Right view

Figure 3: Numerical model of Bridge-Pier-Field-House system.

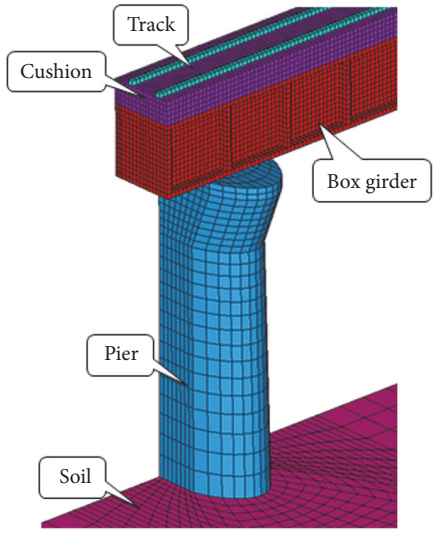

Figure 4: Schematic diagram of each part of the numerical model.

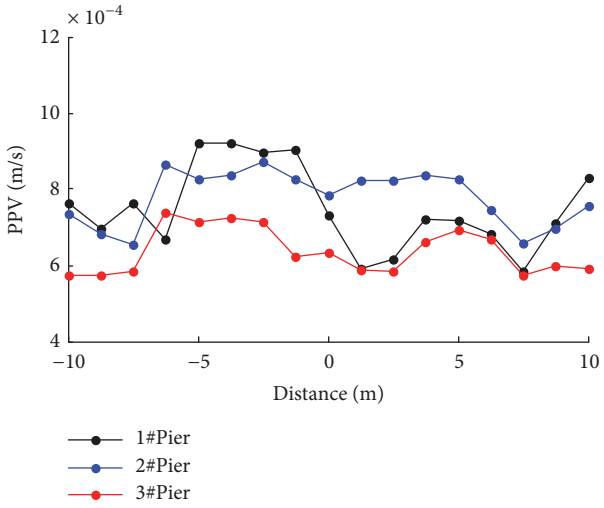

Figure 5: The PPV of points around piers 1#, 2#, and 3#.

3D model mesh contains 226,912 eight-node brick elements. The type of elements which are being used is solid simulating all the part in system. As the structure of the symmetry, in order to reduce the computation, the establishment of a half model simulation. A symmetric boundary condition is introduced into the model at the center of the pier.

The longitudinal direction of the rail and the ballast is restricted to simulate their continuity. As the vibration wave passes through the pier to the soil, it becomes a problem of ground vibration. The whole viaduct system is simplified into two subsystems: the vibration source system (track-cushion-box girder) and the vibration transmission system (pier-residence-soil). The schematic diagram of each part is shown in Figure 4. The elastic parameters of the system material are listed in Table 1. Material damping is modeled using the Rayleigh damping model. The damping ratio is assumed to be 5% in the frequency range of interest.

The propagation of vibration in soil is infinite, and the vibration simulated by FE model is propagated in the boundary of the model. Nonreflecting boundaries are implemented to prevent wave reflections at the edges. The basic principle is to apply viscous normal stress and shear stress on the boundary, which are opposite to the direction of boundary stress, to absorb the energy propagating to the boundary. A study has been done in order to determine the accuracy of nonreflective boundary, comparing the PPV on the test line in Figure 3(a), parallel to the track. Considering the influence of different piers, the center of each pier is taken as the origin, and 17 test points are evenly placed within 20 meters around the pier. The PPV of points around Piers 1#, 2#, and 3# were compared in Figure 5 and the variances of points on the three curves are calculated, respectively. It can be found that the PPV variance of the particles around Pier 1# (which is closer to the boundary) is larger than that of pier 3# (which is farther away from the boundary), the PPV variance of the particles around Pier 3# is 3.613e-9 m/s, and the value is very small. In this paper, the locations of the measured points are all near Pier 3# (Figure 7), which are less affected by the boundary. The analysis results do not depend on the size of the model.

3.2. Simplification of Train Load. According to [26, 27], since the straight railway lines account for a large proportion, only the vertical bearing forces are applied to the Train-Track-Bridge system to solve the ground vibration. For the purpose of comparing the vibration characteristics of computational model and field model, the wheelbase of four-axle wagons and load distribution are stimulated, as shown in Figure 6. Four car bodies are considered, while the actual number can reach more than 100. Using a series of moving loads to represent the effects of the moving train is an alternative for Train-Structure Interaction. The load amplitude takes into account the static wheel load and dynamic load coefficient, and the track irregularity is also taken into account. It has been proved effective in many researches [28, 29]. The train load, which is represented by a series of axles load Pn located in the wheel-track contact points, is formulated with a constant moving speed v. The train load on the track is a one-way pulse stress wave.

In Figure 6, l_c is the wheelbase of the wagon, l_w is the wheelbase of the bogie, l_b is the wheelbase between the bogies, and l_v is the length of a single wagon.

The C64, C70, and C80 track, which are commonly used in China for heavy haul transport, are selected in this numerical model. During the regular arrangement of axle load, vertical loading frequency of wagon mainly depends on wagon speed v (km/h) and wheelbase d (m). When loading frequency is f = v/(3.6·d) and train speed is 80-160 km/ h, the loading frequency of the freight wagon is calculated, as shown in Table 2. It can be seen that the vertical loading frequency of the train is within 26 Hz, and the influence of the wheelbase between bogies and wheelbase inside the bogie on the loading frequency is greater. In the model, the rail is divided into a uniform grid with a side length of 0.2 m. In the calculation, the load time history curve is applied to each unit of the rail. The load curve on each unit is the same but the action time is different. The running speed of the wagon is controlled by

Table 1: Elastic material parameters of the system.

Position	Thickness/ (m)	Density/(kg/m^3)	Modulus of elasticity /(Mpa)	Poisson ratio
Track		7800	6.0E+05	0.22
Cushion	1.0	2200	1.6E+04	0.20
Steel beam	3.0	7800	2.0E+05	0.22
Pier	21.0	2200	2.5E+04	0.20
Layer	8.0	2000	46.62	0.26
Bedrock	∞	2200	2.85E+04	0.20

Table 2: Vertical loading frequency of wagons.

Type of wagon	l_b/m	l_w/m	l_c/m	Wheelbase between wagons/m
C64k	2.988	1.75	6.95	15.19
C70	2.69	1.83	7.38	15.56
C80	1.97	1.83	6.37	13.56
Loading frequency range /Hz	7.44-22.56	12.14-25.39	3.01-6.98	1.46-3.28

the peak rise time and duration time of wheel-rail load curve, and the different axle load is simulated by changing the load amplitude.

3.3. Monitoring Point Arrangement. More measuring points are arranged in the numerical model compared with the field test, which are shown in Figure 7. BP1, BP2, and BP3 are the measuring points of the top of pier, the measuring point at 2 m on the pier from the ground, and the measuring point of pier foundation, respectively. Two vertical lines are placed on the field, Route PL starts from a pier, with eight MPs (No.1 to 8) in horizontal distance of 1.0m, 7.5 m, 15 m, 22.5 m, 30 m, 40 m, 50 m, and 60 m perpendicular to viaduct axis. MR1-MR7 are located at the Route MR. MP1-MP3 are placed on the foundation of the residential building, the center of a room on the ground floor, and the roof, respectively.

3.4. Ground Vibration Analysis. In order to verify the validity of the numerical model, Figure 8 compares the calculated and measured velocity time history and Fourier spectrum of PL3 under C80 running at a speed of 80km/h. The amplitude and trend of velocity time histories are very close between the calculated and measured value, as demonstrated in the figure. Comparison of frequency spectrum shows that the main frequency range of vibration is the same; there is a good correspondence between the calculated and measured results, so the results of numerical simulation are reliable.

Because the horizontal distance between Route PL and the center line is smallest and the horizontal distance between Route MR and the center line is largest, different points on Route PL and Route MR with same distance perpendicular to viaduct axis are selected to observe the attenuation law of vibration on the ground. One case is studied, with available data for C80 with a speed of 80km/h, the change law of root mean square (RMS) velocity vibration level on the two routes is compared. The RMS of a signal is the average of its squared amplitude and is typically calculated over one second interval [30]. The average vibration level and maximum vibration level of different points are shown in Table 3.

As an amplitude descriptor, velocity level L_v is defined as

$$L_V = 20 \lg \left(\frac{V_0}{V_{\text{ref}}} \right), \tag{1}$$

where V_0 is the amplitude of the velocity time history in m/s and V_{ref} is the reference value amplitude 2.54×10^{-8} m/s.

It can be seen from Table 3 obviously that the average vibration level of the measuring point on Route PL is larger than that on Route MR. The attenuation rate of velocity vibration level on Route PL is faster than that on Route MR at the measuring point within 30 m (near source MPs). With the distance from the axle of the viaduct increases from 7.5 m to 30 m, the average vertical vibration level on Route PL decreases from 80.87 dB to 69.56 dB, which decreased 11.31 dB, while the average vertical vibration level on Route MR decreases from 77.85 to 73.11 dB, which decreases by 4.74 dB. The vibration attenuation rate of the Route PL is rapidly first and then slowly with time, which is basically the same as the measured law.

The variation of vertical vibration velocity on either route is analyzed by comparing the RMS velocity level which calculated from (1), as shown in Figure 9. As can be seen, the velocity vibration levels of the measuring points on each route decrease with the increase of distance regularly, but sudden change (suddenly magnified or suddenly reduced) also occurs locally, those regions called the local amplification region (LAR). For example, the average value of vertical velocity vibration levels at 40 m on Route PL is 2.57 dB larger than that at 30 m. This phenomenon had been observed in other field tests [31, 32]. The reason is uncertain; one possible view is that the presence of hard bedrock beneath the soil layer, the wave velocity of the bedrock, is usually larger than that of the surface layer. When the incident wave generated by the vibration source which is reflected and refracted on the surface of bedrock and the surface wave propagating along the ground surface reaches a certain point on the ground at the same time, the superposition of the waves will form a local amplification.

Table 3: Maximum and average velocity levels at different routes (dB).

		Vertical vibration				Horizontal vibration			
		Route PL		Route MR		Route PL		Route MR	
		Max	Average	Max	Average	Max	Average	Max	Average
MPs	7.5	94.99	80.87	85.93	74.85	93.52	80.47	87.49	75.96
	15	88.29	74.01	81.0	71.31	84.58	73.78	85.07	72.85
	22.5	83.32	72.55	84.48	71.54	85.06	74.36	82.93	70.18
	30	80.62	69.56	82.98	70.11	73.98	63.07	84.49	71.78
	40	**82.17**	**72.13**	**78.62**	**67.22**	**77.99**	**66.86**	**74.72**	**64.61**
	50	80.09	68.62	72.87	62.51	78.61	66.72	74.31	62.86
	60	74.81	64.95	69.03	59.00	76.17	66.20	73.49	61.69

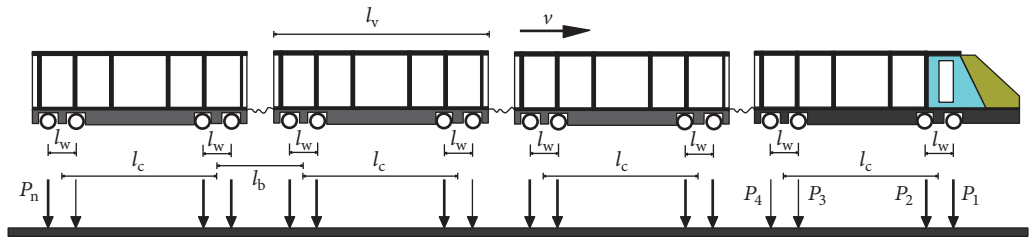

Figure 6: The layout and geometrical specification of wagons.

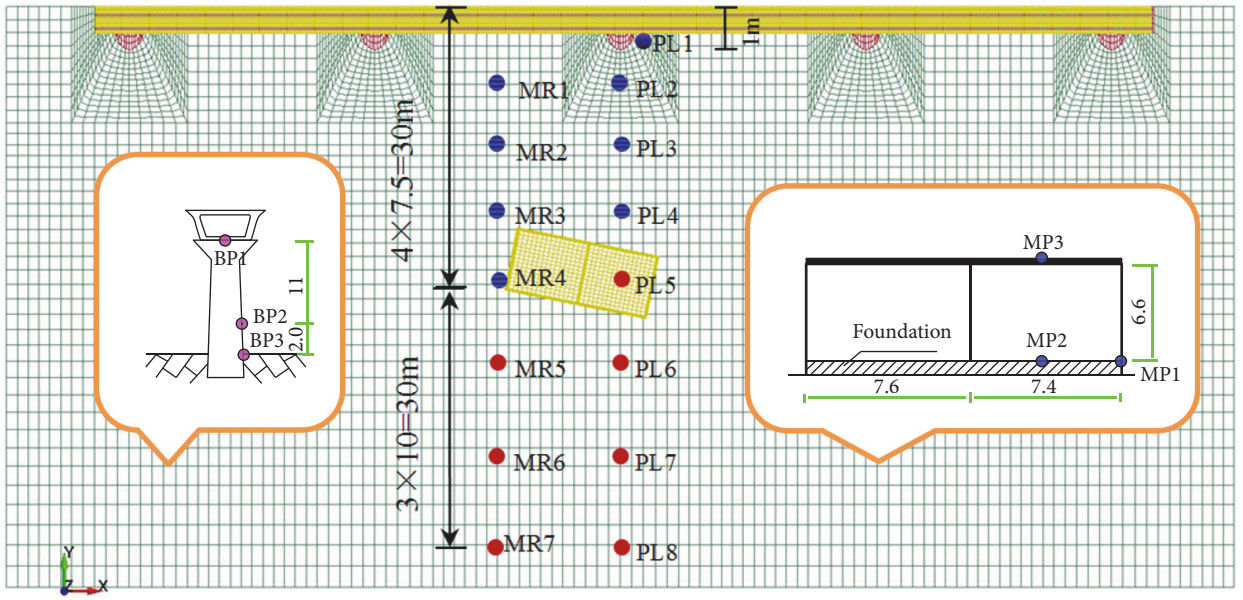

Figure 7: Layout of measuring points in the numerical model (unit: m).

Figure 10 displays the horizontal and vertical velocity of all the points on Rout PL introduced previously (Section 3.3) in the form of one-third center frequency band within the scope of 1-80Hz. Due to the vibration-absorbing effect of soil, the vibration usually decreases with the increase of the distance, but there are exceptions in some frequency bands, like vertical vibration at 7.5m which is obviously larger than that at 1.0m in 25Hz to 35Hz frequency bands. The measuring point within 30m has an amplification phenomenon at the center frequency of 8~16Hz and 20~25Hz, and the amplification is only obvious near the center frequency of 10Hz beyond 30m. The frequency less than 8 Hz is rapidly attenuated from 1 m to 7.5 m and then remains stable. However, the frequency band above 20 Hz is uniformly attenuated with distance. It indicates that vibration in frequency between 8 and 16 Hz, where PPV lies, attenuates at a lower rate. It is an interesting phenomenon that no much attenuation is observed for distances larger than 30 m; the higher frequencies of the ground vibration wave attenuate fast, while the lower frequencies attenuate slowly. Higher frequencies at

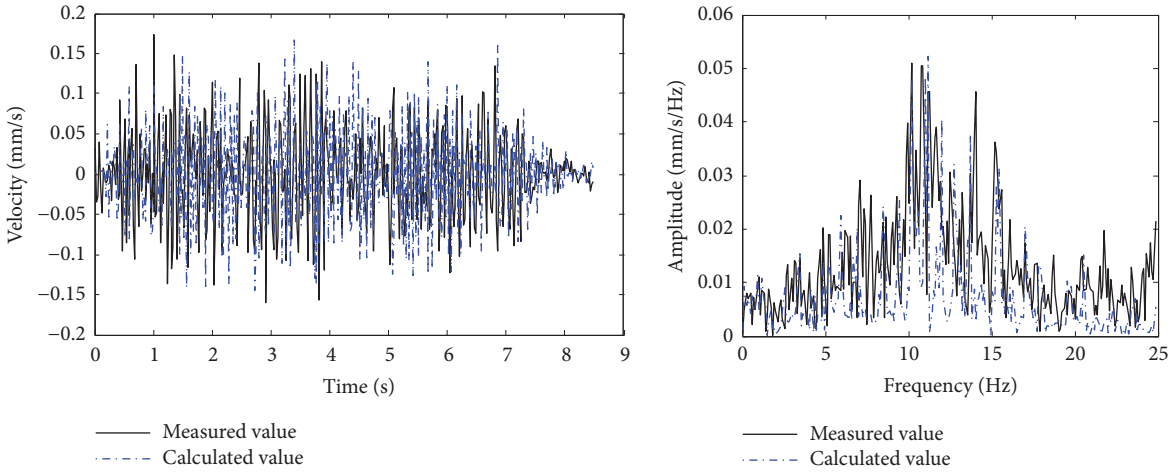

Figure 8: Comparison of calculated and measured values of velocity time and spectrum of ground point.

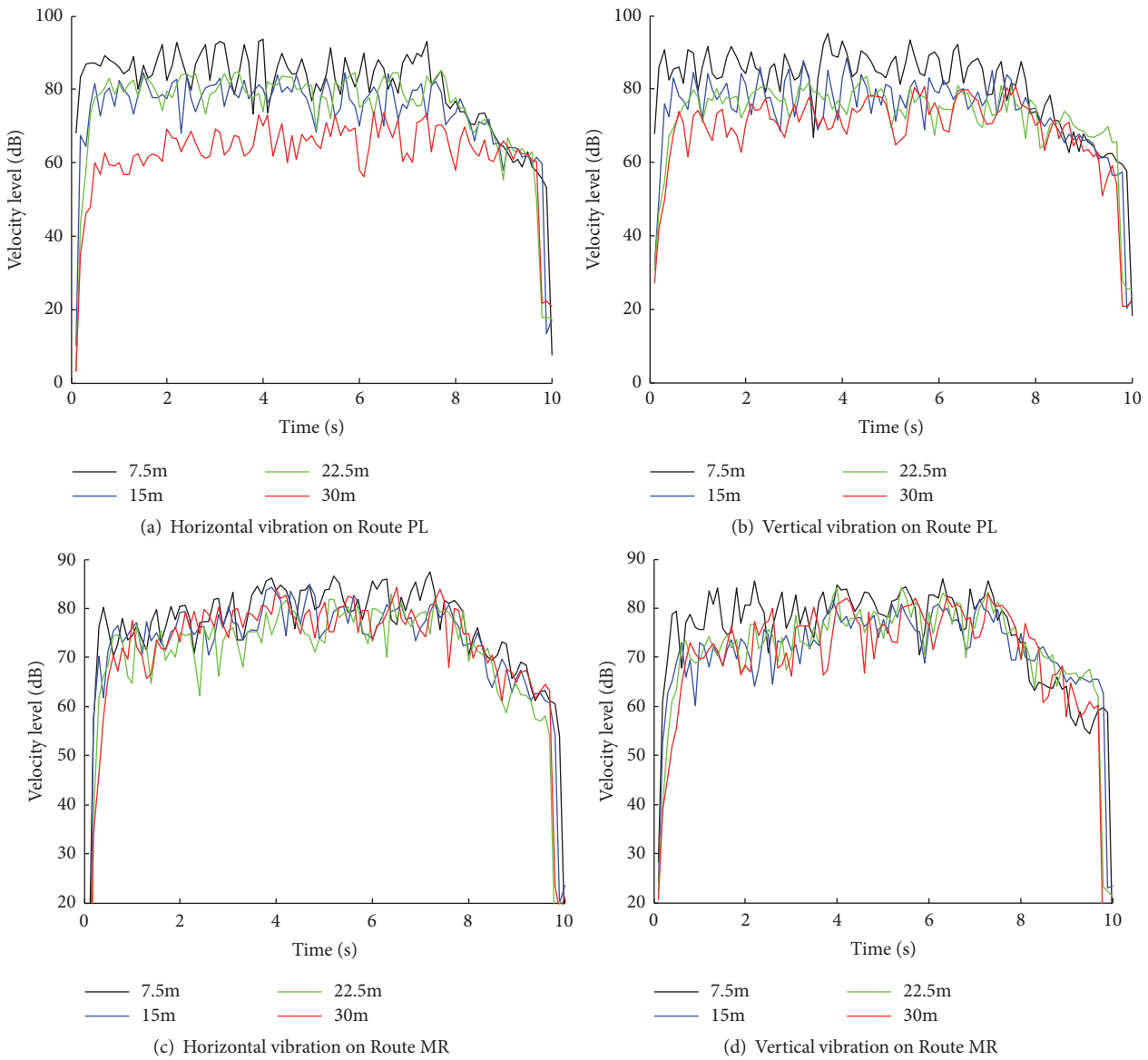

Figure 9: The attenuation law of vibration on different route.

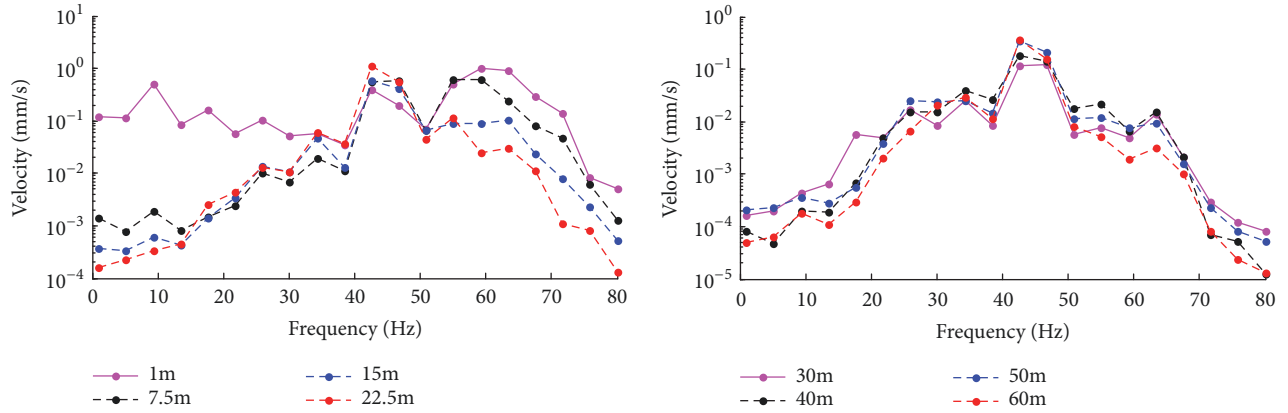

(a) Horizontal vibration

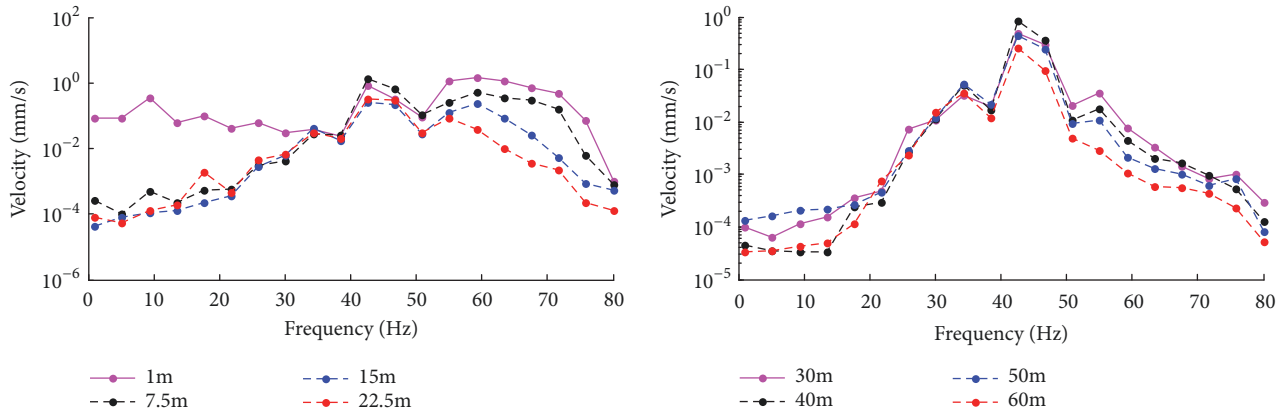

(b) Vertical vibration

Figure 10: The effective value of 1/3 octave band velocity on Route PL.

distances larger than 30 m have been attenuated more than half (perhaps 80 percent). On the other hand, Rayleigh wave will play a leading role in the far field which accounts for 67% of the total energy. The attenuation speed of Rayleigh wave is much slower than that of body wave, so the attenuation of vibration is slower at distances larger than 30 m.

4. Regression Analysis Using Sodev's Modified Formula

Propagation characteristics of vibrations generated by various vibration sources may be dependent on the type of the generated waves which can be assessed by measuring particle motions. According to the analysis of the literature, the magnitude of the dynamic load transmitted to the ground by the pier is mainly affected by the train running speed and axle weight. After the vibration wave is transmitted to the soil through the pier, it is converted into the ground vibration problem purely under the point source excitation condition. It is similar to the vibration effect induced by blasting in the middle and far region. In fact, the propagation medium of blasting vibration and pier vibration caused by wagons are both rock and soil mass, and the vibration of medium near the protected object is elastic vibration. The relationship between the PPV and the distance to vibration source can be described by the modified Sodev's formula, as shown in (2) to (4).

$$V_{peak} = k' \left(\frac{\sqrt[3]{Q'}}{D} \right)^{\alpha'}, \tag{2}$$

$$V_{peak} = k'' D^{-\alpha'}, \tag{3}$$

$$k'' = k' \left(Q'^{\alpha'/3} \right), \tag{4}$$

where k' and α' are the coefficients related to local geological condition, Q' is a comprehensive indicator considering various factors which affect the source of energy (hereinafter referred to as the energy index), and D is the scaled distance. For vibration source, two adjustments are applied including the train type and train speed.

In this section, the following steps are taken to obtain the PPV of the ground point which is d from the center of the pier according to (2): (1) Referring to the method of determining site coefficient in blasting, k' and α' are obtained. (2) When the wagon weight is the same, multiple sets of data are used for regression analysis based on the (3), and then k'' is got and it is substituted in (4) to get Q' at different wagon speeds,

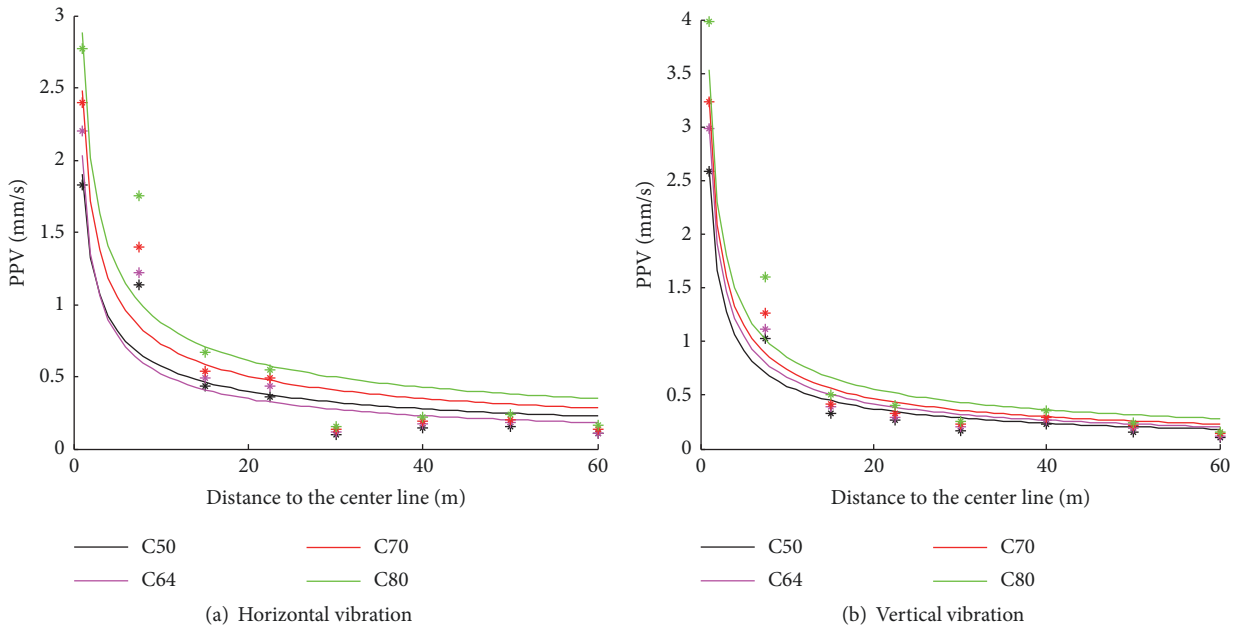

Figure 11: Power function fitting of PPV under different wagon weights.

and the change law of Q' with the wagon speed can be fitted by least square method. (3) In the same way as step (2), the relationship between Q' and wagon weight at the same speed can be fitted. (4) Repeat steps (2) and (3); multiple sets of change law of Q' with wagon speed and Q' with wagon weight are obtained, so as to fit the calculation equation of Q' under any wagon speed and wagon weight. (5) After Q' is obtained, substitute it into (2) to obtain the PPV at any point.

4.1. PPV and Wagon Weight. A total of four types of trains (between C50 and C80) were analyzed in the model, and the values of k'' and α' in (3) are discussed when the train speed is 80km/h. The fitting result between PPV and distance to the center line (D) of each MPs on Rout PL is shown in Table 4. Figure 11 shows the relationship curves between PPV and distance under different wagon weights.

As can be seen from Table 4 and Figure 11, the correlation coefficients in the fitting equation (3) are all greater than 88% and the mean square error (MSE) is less than 0.8. The fitting accuracy of vertical vibration is higher than that of horizontal vibration. It is verified that the relationship between PPV and distance under different wagon weights conforms to power function. The coefficient k'' varies greatly with the increase of the total weight of the wagon. For the horizontal vibration, from C50 to C80, k'' gradually increases from 1.901 to 2.887, and α' maintains at around 0.5. For vertical vibration, k'' gradually increases from 2.612 to 3.533 and α' maintains around 0.65, indicating that the weight of the wagon has a great influence on the PPV, especially the near-source measuring point.

4.2. PPV and Wagon Speed. Taking the fully loaded train C80 as an example, a total of five speeds (between 80 and 160 km/h) were analyzed in the section. Table 5 and Figure 12 present the fitting result of PPV and D on Rout PL at different wagon speeds according to formula (3).

It can be seen from Table 5 and Figure 12 that the correlation coefficients in fitting equation (3) are all greater than 85% and the MSE are less than 0.9754. As wagon speed increases, the coefficient k'' increases, and k'' in the vertical vibration is larger than that in horizontal vibration, while α is relatively stable. When the wagon speed increases from 80km/h to 160km/h, for horizontal vibration, k'' gradually increases from 2.887 to 3.666, and for vertical vibration, k'' gradually increases from 3.533 to 8.896. With the increase of wagon speed, the increasing speed of PPV at the same point slows down.

4.3. Determination of Site Coefficient. The blasting vibration simulation was carried out on the site of the model to determine the value of site coefficient. Piers in the original model were removed, and the equivalent blasting load was applied in hole of the pier. A simplified triangular load curve is adopted, as shown in Figure 13. Among them, P_w is the peak pressure of blasting, t_1 is boost time, and t_2 is total action time.

The boost time is set to 2 ms, total action time is set to 7 ms, the total calculation time is 300 ms, and the peak pressure of the blasting equivalent load is 6.64 MPa when the charge is 120 kg. The velocity time histories of particles at different distances on the site are extracted by calculation, and the relationship between the PPV of the measuring points and the distance from blasting center is fitted by Sodev's formula (see (5)).

$$V_{peak} = k\left(\frac{\sqrt[3]{Q}}{D}\right)^{\alpha}, \tag{5}$$

Table 4: Fitting of PPV versus distance under different wagons.

Vibration Component	Wagon	k''	α'	Correlation coefficient	MSE
Horizontal	C50	1.901	0.5219	0.885	0.3154
	C64	2.036	0.5914	0.9504	0.1512
	C70	2.48	0.5318	0.9046	0.4369
	C80	2.887	0.5181	0.8783	0.7745
Vertical	C50	2.612	0.6494	0.9708	0.1472
	C64	3.021	0.6576	0.9743	0.1477
	C70	3.267	0.6474	0.9736	0.2071
	C80	3.533	0.6163	0.965	0.3188

Table 5: Fitting of PPV versus distance under different speeds.

Vibration Component	Speed/(km/h)	k''	α'	Correlation coefficient	MSE
Horizontal	80	2.887	0.5181	0.8783	0.7745
	100	3.109	0.4915	0.8581	0.8791
	120	3.434	0.4191	0.8742	0.9754
	140	3.580	0.4452	0.8825	0.8615
	160	3.666	0.4097	0.9252	0.5892
Vertical	80	3.533	0.6163	0.9650	0.3188
	100	3.644	0.5465	0.9745	0.2282
	120	4.082	0.4987	0.9607	0.4268
	140	4.275	0.4691	0.9856	0.1549
	160	4.896	0.4642	0.9775	0.3131

where k and α are site coefficients; Q is the mass of the blasting single-shot explosive (kg). Formula (5) takes logarithms on both sides simultaneously

$$\ln V_{peak} = \ln k + \alpha \ln\left(\frac{\sqrt[3]{Q}}{D}\right), \tag{6}$$

where $y = \ln V_{peak}$, $x = \ln(\sqrt[3]{Q}/D) = (1/3)\ln Q - \ln D$, and $b = \ln k$.

Equation (6) becomes the following linear form:

$$y = \alpha x + b. \tag{7}$$

By means of linear regression with the above method, when the MSE of calculated value and fitted value are the smallest, the coefficients α and b are obtained. Results are as follows, in horizontal direction, α=1.447, b=4.056, k=57.74 and in vertical direction, α=1.479=1.479, b=3.351, k=28.53.

The site coefficients are substituted into Equation (3), k_x'' represents horizontal direction, and k_z'' represents vertical direction

$$\begin{aligned} k_x'' &= 57.74 * \left(\mathrm{Q}'^{0.482}\right) \\ k_z'' &= 28.53 * \left(\mathrm{Q}'^{0.493}\right) \end{aligned} \tag{8}$$

4.4. Prediction Formula of PPV. If to predict PPV by (2), after site coefficients are calculated, the energy index Q' is also needed. The following two regression methods are used to analyze the relationship between energy index and wagon speed and wagon weight.

(a) Linear Regression. According to the corresponding value of k'' at the same speed and different weight in Table 4, Q' corresponding to each weight can be obtained by substituting them in (8); results are shown in Table 6. Making linear fitting between energy index and total weight of wagon, the fitting formula is shown in (9)

$$Q'(g) = a_1 g + b_1, \tag{9}$$

where g is total weight of wagon in t; a_1 and b_1 are linear fitting coefficient.

Fitting results show that fitting correlation coefficient in fitting equation (9) is greater than 90% and the max difference value (D-value) percentage between the fitting value and the calculated value is 6.36%, D-value in vertical direction are all less than 1%. Among them, the linear fitting coefficients of horizontal direction are a_1=5.47×10^{-7} and b_1=-2.689×10^{-5}, while those of vertical direction are a_1=1.768×10^{-6} and b_1=-5.022×10^{-5}. According to (9), the Q' values of different wagon weights can be estimated under the same site condition and wagon speed.

According to similar method above, using the value of k'' at same weight and different speeds in Table 5, Q' corresponding to each speed can be obtained in Table 7. Making linear fitting between energy index and wagon speed, the fitting formula is shown in (10)

$$Q'(v) = c_1 v + d_1, \tag{10}$$

where v is wagon speed in km/h; c_1 and d_1 are linear fitting coefficient.

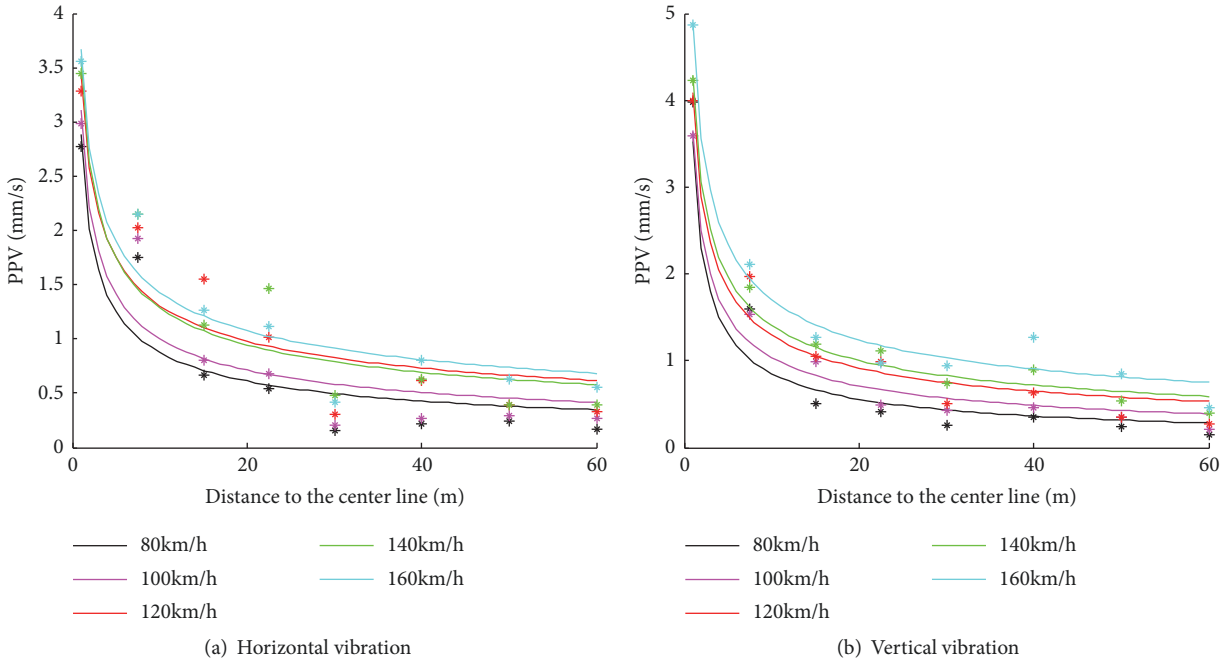

Figure 12: Power function fitting of PPV under different speeds.

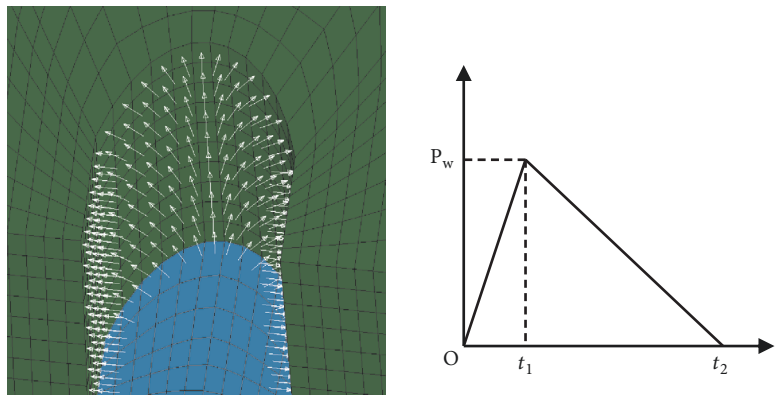

Figure 13: Applied blasting load.

Table 6: Energy index values under different wagon weight.

Type of wagon	Total weight /(t)	Horizontal		Vertical	
		Q' (10-5)	D-value	Q' (10-4)	D-value
C50	70	1.363	6.36%	0.734	0.19%
C64	84	1.572	6.23%	0.926	0.31%
C70	94	2.366	3.67%	1.126	0.32%
C80	105	3.242	5.78%	1.355	0.059%

Table 7: Energy index values under different wagon speed.

Type of wagon	Speed /(km/h)	Horizontal		Vertical	
		Q' (10-5)	D-value	Q' (10-4)	D-value
C80	80	3.242	2.47%	1.355	6.33%
C80	100	3.78	2.48%	1.443	3.6%
C80	120	4.645	4.56%	1.817	1.69%
C80	140	5.064	2.17%	1.995	5.14%
C80	160	5.32	3.35%	2.626	3.06%

The fitting results show that energy index increases linearly with the train speed between 80 km/h and 160km/h; the D-value percentage between fitting value and calculated value is all less than 8%. Among them, the linear fitting coefficients of horizontal direction are c_1=2.72×10^{-7} and d_1=1.146×10^{-5}, while those of vertical direction are c_1=1.158×10^{-6} and d_1=-0.981×10^{-6}. The Q' value in vertical is larger than horizontal, which indicates that the increase of train speed has a greater impact on vertical vibration. According to (10), the Q' values of different wagon speeds can be estimated.

According to (9) and (10), Q' is both the function of wagon weight and wagon speed. Therefore, Q' is assumed to have the following forms for it has a linear relationship both with wagon weight and wagon speed.

$$\begin{aligned} Q'(v,g) &= (A_1 v + B_1)\, g + (A_2 v + B_2) \\ &= (A_1 g + A_2)\, v + (B_1 g + B_2), \end{aligned} \tag{11}$$

where A_1, B_1 and A_2, B_2 are fitting coefficients. At a specific speed, the form of Q' is as follows:

$$\begin{aligned} Q'(80,g) &= a_1 g + b_1 \\ Q'(100,g) &= a_2 g + b_2 \\ &\vdots \\ Q'(v,g) &= a_{vn} g + b_{vn}, \end{aligned} \tag{12}$$

The values of a_1 and b_1 have been solved above, and the same method can be used to find out the value of $a_2, b_2 \ldots a_{vn}, b_{vn}$. According to (11), regression coefficient $a_1, a_2 \cdots a_{vn}$ and $b_1, b_2 \cdots b_{vn}$ have linear relationship with wagon speed respectively, it is expressed in the form as

$$\begin{aligned} a_{vn} &= A_1 v + B_1 \\ b_{vn} &= A_2 v + B_2, \end{aligned} \tag{13}$$

The coefficients of A_1, B_1 and A_2, B_2 were calculated by fitting $a_1, a_2 \cdots a_{vn}$, $b_1, b_2 \cdots b_{vn}$ and speed, respectively, and then the change law of Q' with wagon speed and wagon weight can be found by substituting them in (11).

(b) Nonlinear Regression. Volberg's [21] study has shown the logarithmic relationship between ground vibration velocity level caused by trains and train speed in a certain frequency range in 1983.

$$L_v = 64 + 20 \lg\left(\frac{v}{40}\right), \tag{14}$$

where v is the wagon speed in km/h, L_V is vibration velocity level in dB. From (14), it can be seen that the velocity vibration level is logarithmic with the wagon speed, while from (1), it can be seen that the velocity vibration level is logarithmic with PPV, then it can be deduced that there is a linear relationship between PPV and wagon speed. According to (2), the relationship between Q' and PPV can be deduced.

$$Q' = \left(\frac{V_{peak}}{k'}\right)^{3/\alpha'} \cdot D^3, \tag{15}$$

Assuming the linear relationship between PPV and wagon speed, the relationship between Q' and wagon speed can be assumed as follows:

$$Q' = (p_1 \cdot v + p_2)^{3/\alpha'}, \tag{16}$$

where p_1 and p_2 are linear fitting coefficient; α' is coefficient for site condition. Wagon speed and corresponding Q' values in Table 7 are regression analyzed according to (16). The results are compared with linear regression, as shown in Figure 14.

The nonlinear fitting coefficients in horizontal direction are obtained like p_1=2.463×10^{-5} and p_2=0.0049, while the nonlinear fitting coefficients in vertical direction are p_1=5.668×10^{-5} and p_2=0.0075. As can be seen from Figure 14, results of Q' under different wagon speed calculated by the two methods are very close, the RMS in vertical direction of the two fitting methods are compared with numerical value, the nonlinear fitting is 1.206×10^{-6}, and the linear fitting is 1.232 ×10^{-6}.

A similar method is used to fit the relationship between Q' and wagon weight, assuming the relationship between them is as follows:

$$Q' = (q_1 \cdot g + q_2)^{3/\alpha'}. \tag{17}$$

The wagon weight and corresponding Q' values in Table 6 are regression analyzed according to (17). Results are compared with the linear regression, as shown in Figure 15.

The nonlinear fitting coefficients in horizontal direction are obtained like q_1=6.414×10^{-5} and q_2=-1.64×10^{-4}, while nonlinear fitting coefficient in vertical direction are q_1=9.23×10^{-5} and q_2=0.0027. As shown in Figure 15, the nonlinear fitting is more accurate, for the RMS in the vertical direction by the nonlinear fitting is 6.427×10^{-6}, and is smaller that of the linear fitting which is 6.515 ×10^{-6}.

When wagon speed and wagon weight are both variables, the expression of Q' which satisfied (16) and (17) is as follows:

$$\begin{aligned} Q'(g,v) &= \left[(P_1 g + Q_1)\, v + (P_2 g + Q_2)\right]^{3/\alpha'} \\ &= \left[(P_1 v + P_2)\, g + (Q_1 v + Q_2)\right]^{3/\alpha'} \end{aligned} \tag{18}$$

where P_1, Q_1, and P_2, Q_2 are fitting coefficients. When wagon speed is the same, the forms of Q' under different wagon weights are as follows:

$$\begin{aligned} Q'(80,g) &= (q_1 g + q_2)^{\alpha'/3} \\ Q'(100,g) &= (q_{21} g + q_{22})^{\alpha'/3} \\ &\vdots \\ Q'(v_n,g) &= (q_{n1} g + q_{n2})^{\alpha'/3}. \end{aligned} \tag{19}$$

The value of q_1 and q_2 have been solved above, and the same method can be used to find out the value of $q_{21}, q_{22} \ldots q_{n1}, q_{n2}$. The regression coefficients $q_1, q_{21} \cdots q_{n1}$

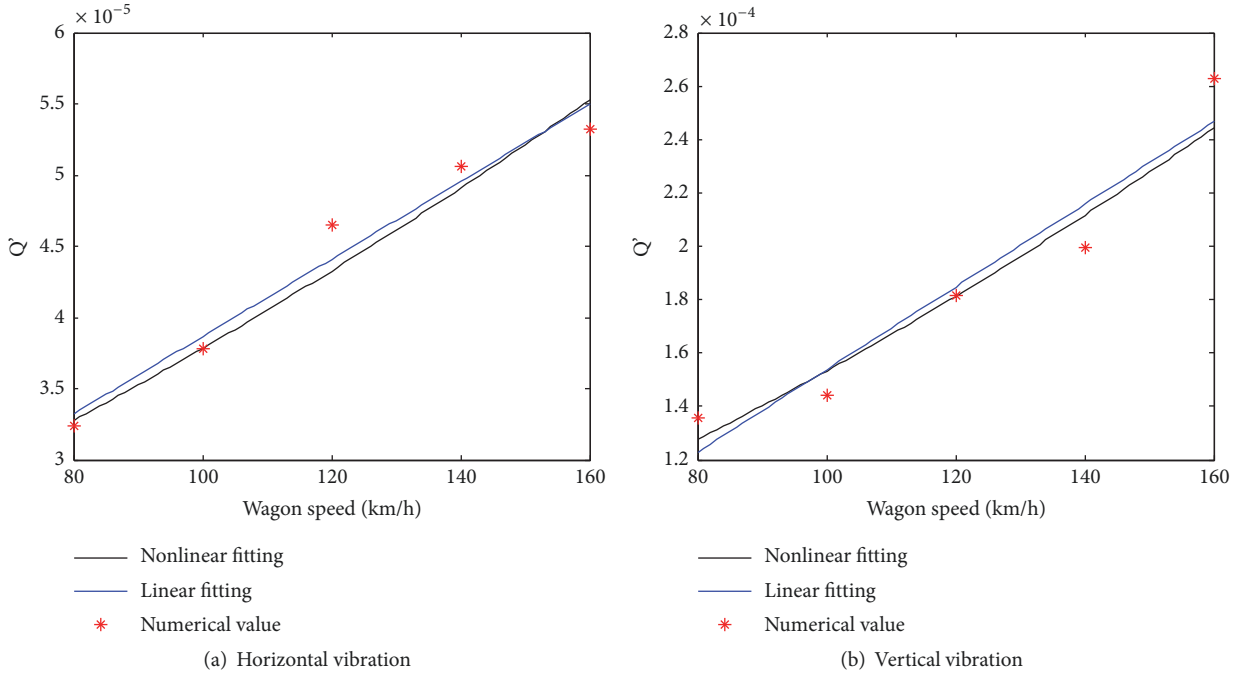

Figure 14: Regression analysis of energy index Q' and wagon speed.

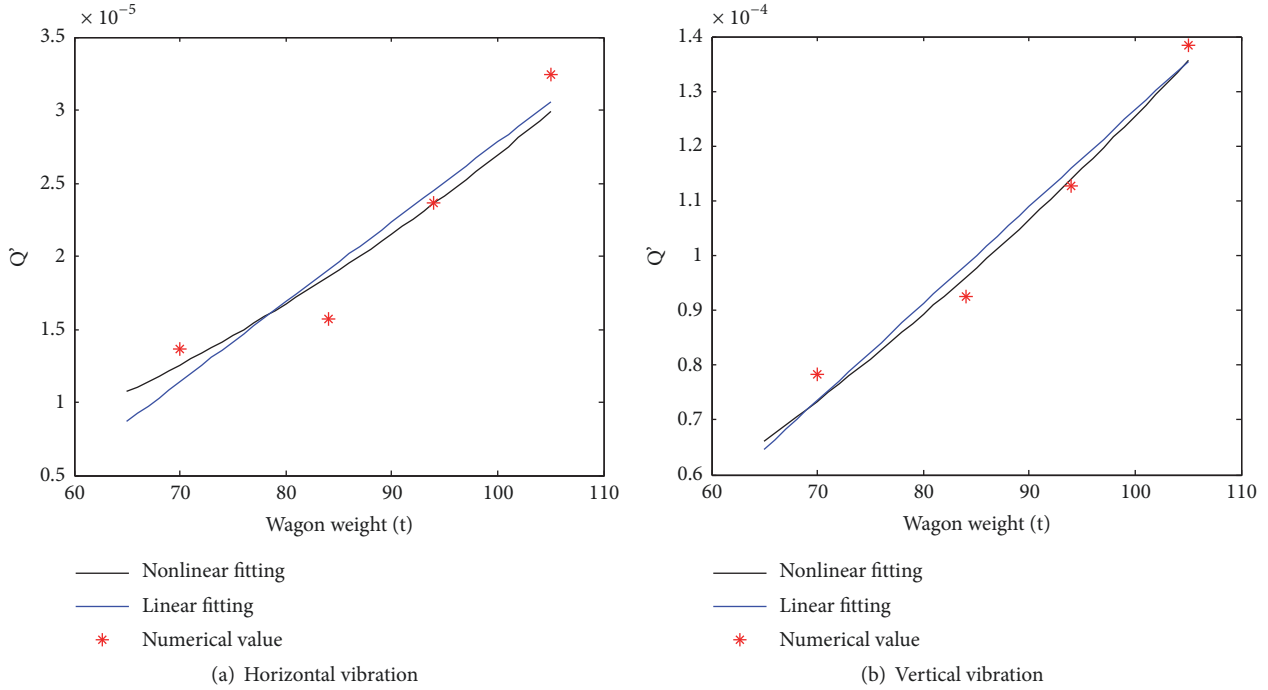

Figure 15: Regression analysis of energy index Q' and wagon weight.

and $q_2, q_{22} \cdots q_{n2}$ both have linear relationship with wagon speed, respectively; according to (18), it is expressed in the form as follows:

$$q_{n1} = P_1 v + P_2$$
$$q_{n2} = Q_1 v + Q_2. \tag{20}$$

The coefficients P_1, P_2, and Q_1, Q_2 were calculated by fitting $q_1, q_{21} \cdots q_{n1}$, $q_2, q_{22} \cdots q_{n2}$ and wagon speed, respectively, and then we can obtain the functional expression of Q' by substituting them in (18). Setting Q' into (2), PPV of any surface point at different speed and wagon weight can be obtained.

Table 8: Comparison of PPV of measuring points (mm/s).

Location of MPs /m	Measured value		Numerical value		Linear fitting Value		Nonlinear fitting value	
	Horizontal	Vertical	Horizontal	Vertical	Horizontal	Vertical	Horizontal	Vertical
1	1.762	2.732	1.803	2.7296	2.01	3.01	1.96	2.97
7.5	0.869	1.212	0.8269	1.2654	0.798	1.118	0.789	1.08
15	0.304	0.402	0.3287	0.4113	0.377	0.418	0.352	0.412
22.5			0.2639	0.3326	0.281	0.368	0.285	0.355

4.5. Comparison of Fitting Result and Monitoring Result. When full C64 is running at 100km/h on the viaduct, the monitoring results, numerical results, and fitting results of the PPV of four MPs with the distance between MPs and center line are 1, 7.5, 15, and 22.5m which are shown in Table 8.

It is found that the PPV at 15m is less than 0.5mm/s; the ground vibration caused by wagons running on viaducts decreases rapidly with the increase of distance. Compared with PPV of MPs, the numerical value is close to the measured value, which verifies the correctness of the numerical model. Comparing the numerical value with the predicted value by two regression methods, it is obvious that the nonlinear fitting value is closer to the numerical value. Although the fitting value at 7.5m is smaller and the value at 15m is slightly larger, the deviation is less than 8%, which can predict the attenuation trend of ground point vibration basically.

5. Conclusion

In this paper, the ground vibration attenuation rule and propagation law are systematically discussed by establishing the numerical model of Shenshan viaduct and its surrounding site. Based on the modified Sadev's formula, the prediction formulas of PPV under different wagon speeds and axle loads are proposed by linear regression and nonlinear regression respectively. Method to determine each parameter in the prediction formula is discussed; on the basis of the simulation results, the principal conclusions (may be confined to the similar configurations as this paper) are as follows:

(1) The comparison between numerical and measured results revealed a good agreement, which confirms the integrated Bridge-Pier-Field-House model established in this paper is consistent with the actual project and can reflect the vibration propagation chain caused by train passing through viaduct.

(2) In the site, the attenuation of velocity vibration level of the MPs on Route PL is faster than MPs on Route MR; moreover, the velocity vibration level of the MPs on Route PL shows a power function attenuation trend with the increase of distance. However, there will also have the amplification regions (LAR); the positions and quantities of LAR are different in different directions.

(3) The prediction formula proposed in the paper can predict the PPV of ground vibration under different train speeds, axle loads, and site conditions effectively. Comparing the fitting value with numerical calculation values, except that the result at 7.5m is smaller, other results are close, which verifies the correctness of the prediction method.

(4) The concept of energy index Q' is proposed in prediction formula firstly; the relationship between energy index, axle load, and speed is regressed by linear fitting and nonlinear fitting. The results show that the values obtained by nonlinear fitting are more accurate.

The prediction formula presented in this paper does not consider the mutation phenomenon in the attenuation process, and the more accurate formula needs to be studied further under more cases.

Data Availability

The data used to support the findings of this study are available from the corresponding author upon request.

Conflicts of Interest

The authors declare no conflicts of interest in preparing this article.

Acknowledgments

This work supported by the National Natural Science Foundation of China (51779197 and 51378500).

References

[1] D. P. Connolly, G. Kouroussis, P. K. Woodward, P. Alves Costa, O. Verlinden, and M. C. Forde, "Field testing and analysis of high speed rail vibrations," *Soil Dynamics and Earthquake Engineering*, vol. 67, pp. 102–118, 2014.

[2] D. P. Connolly, P. A. Costa, G. Kouroussis, P. Galvin, P. K. Woodward, and O. Laghrouche, "Large scale international testing of railway ground vibrations across Europe," *Soil Dynamics and Earthquake Engineering*, vol. 71, pp. 1–12, 2015.

[3] W. Zhai, K. Wei, X. Song, and M. Shao, "Experimental investigation into ground vibrations induced by very high speed trains on a non-ballasted track," *Soil Dynamics and Earthquake Engineering*, vol. 72, pp. 24–36, 2015.

[4] H. Xia and N. Zhang, "Dynamic analysis of railway bridge under high-speed trains," *Computers & Structures*, vol. 83, no. 23-24, pp. 1891–1901, 2005.

[5] L. Liu, C. Tao, R. Sun, H. Chen, and Z. Lin, "Non-stationary channel characterization for high-speed railway under viaduct scenarios," *Chinese Science Bulletin*, vol. 59, no. 35, pp. 4988–4998, 2014.

[6] J. M. Olmos and M. A. Astiz, "Analysis of the lateral dynamic response of high pier viaducts under high-speed train travel," *Engineering Structures*, vol. 56, pp. 1384–1401, 2013.

[7] S. Kusuhara, S. Fukunaga, and N. Toyama, "Reevaluation of aerodynamic stability for the Tozaki viaduct," *Kozo Kogaku Ronbunshu A*, vol. 56, pp. 608–615, 2010.

[8] I. Nakaya, K. Hayakawa, T. Nishimura, and K. Tanaka, "The long distance propagation mechanism of environmental ground vibration due to the viaduct," *Journal of Japan Society of Civil Engineers Ser C*, vol. 65, pp. 196–212, 2009.

[9] P. Li, X. Ling, F. Zhang, Y. Li, and Y. Zhao, "Field testing and analysis of embankment vibrations induced by heavy haul trains," *Shock and Vibration*, vol. 2017, Article ID 7410836, 14 pages, 2017.

[10] L. Pugi, D. Fioravanti, and A. Rindi, "Modelling the longitudinal dynamics of long freight trains during the braking phase," in *Proceedings of the 2th Iftomm World Congress*, pp. 18–21, Micropolis Congress Center, Besançon, France, 2007.

[11] L. Pugi, A. Palazzolo, and D. Fioravanti, "Simulation of railway brake plants: An application to SAADKMS freight wagons," *Proceedings of the Institution of Mechanical Engineers, Part F: Journal of Rail and Rapid Transit*, vol. 222, no. 4, pp. 321–329, 2008.

[12] N. Correia dos Santos, J. Barbosa, R. Calçada, and R. Delgado, "Track-ground vibrations induced by railway traffic: experimental validation of a 3D numerical model," *Soil Dynamics and Earthquake Engineering*, vol. 97, pp. 324–344, 2017.

[13] P. Alves Costa, R. Calçada, and A. Silva Cardoso, "Track–ground vibrations induced by railway traffic: In-situ measurements and validation of a 2.5D FEM-BEM model," *Soil Dynamics & Earthquake Engineering*, vol. 32, no. 1, pp. 111–128, 2012.

[14] A. H. Mohammad, N. A. Yusoff, A. Madun et al., "Ground vibration attenuation measurement using triaxial and single axis accelerometers," *Journal of Physics: Conference Series*, p. 012113, 2018.

[15] A. M. Kaynia, F. Løvholt, and C. Madshus, "Effects of a multilayered poro-elastic ground on attenuation of acoustic waves and ground vibration," *Journal of Sound and Vibration*, vol. 330, no. 7, pp. 1403–1418, 2011.

[16] Q. Liu, X. Zhang, Z. Zhang, and X. Li, "In-situ measurement of ground vibration induced by inter-city express train," *Applied Mechanics and Materials*, vol. 204-208, pp. 502–507, 2012.

[17] G. Kouroussis, G. Alexandrou, J. Florentin, and O. Verlinden, "Prediction of railway-induced ground vibrations: The use of minimal coordinate method for vehicle modelling," *Notes on Numerical Fluid Mechanics and Multidisciplinary Design*, vol. 126, pp. 329–336, 2015.

[18] P. Vanhonacker and H. Masoumi, "Mitigation of ground vibrations from freight trains," in *Proceedings of the Transport Research Arena (TRA) 5th Conference: Transport Solutions from Research to Deployment*, The National Academies of Sciences, Engineering, and Medicine, Paris, France, 2014.

[19] I. G. Lombaert, S. Lombaert, G. Grande, G. Lombaert, G. Degrande, and D. Clouteau, "Road traffic induced free field vibrations: numerical modelling and in situ measurements," in *Proceedings of the International Workshop Wave 2000, Wave propagation, Moving load, Vibration reduction*, pp. 195–207, A. A. Balkema, Rotterdam, Netherlands, 2000.

[20] D. I. G. Bornitz, *Über die Ausbreitung der von Großkolbenmaschinen Erzeugten Bodenschwingungen in die Tiefe*, Springer, Berlin, Germany, 1931.

[21] G. Volberg, "Propagation of ground vibrations near railway tracks," *Journal of Sound and Vibration*, vol. 87, no. 2, pp. 371–376, 1983.

[22] J.-G. Chen, H. Xia, and Y.-M. Cao, "Analysis and prediction on environmental vibration induced by elevated rail transit," *Gongcheng Lixue/Engineering Mechanics*, 2012.

[23] M. Hajihassani, D. Jahed Armaghani, A. Marto, and E. Tonnizam Mohamad, "Ground vibration prediction in quarry blasting through an artificial neural network optimized by imperialist competitive algorithm," *Bulletin of Engineering Geology and the Environment*, vol. 74, no. 3, pp. 873–886, 2015.

[24] H. Dehghani and M. Ataee-pour, "Development of a model to predict peak particle velocity in a blasting operation," *International Journal of Rock Mechanics and Mining Sciences*, vol. 48, no. 1, pp. 51–58, 2011.

[25] T. Mokfi, A. Shahnazar, I. Bakhshayeshi, A. M. Derakhsh, and O. Tabrizi, "Proposing of a new soft computing-based model to predict peak particle velocity induced by blasting," *Engineering with Computers*, vol. 34, no. 4, pp. 881–888, 2018.

[26] Y.-S. Wu and Y.-B. Yang, "A semi-analytical approach for analyzing ground vibrations caused by trains moving over elevated bridges," *Soil Dynamics and Earthquake Engineering*, vol. 24, no. 12, pp. 949–962, 2004.

[27] X. Li, Z. Zhang, and X. Zhang, "Using elastic bridge bearings to reduce train-induced ground vibrations: An experimental and numerical study," *Soil Dynamics and Earthquake Engineering*, vol. 85, pp. 78–90, 2016.

[28] K. Liu, E. Reynders, G. D. Roeck, and G. Lombaert, "Experimental and numerical analysis of a composite bridge for high-speed trains," *Journal of Sound and Vibration*, vol. 320, no. 1-2, pp. 201–220, 2009.

[29] S.-J. Feng, X.-L. Zhang, Q.-T. Zheng, and L. Wang, "Simulation and mitigation analysis of ground vibrations induced by high-speed train with three dimensional FEM," *Soil Dynamics and Earthquake Engineering*, vol. 94, pp. 204–214, 2017.

[30] I. Duvnjak, L. Herceg, and M. Rak, "Experimental investigation of railway train-induced ground vibration," in *Proceedings of the 28th Danubia-Adria-Symposium on Advances in Experimental Mechanics, DAS 2011*, Scientific Society for Mechanical Engineering, Siófok, Hungary, October 2011.

[31] T. Fujikake, "A prediction method for the propagation of ground vibration from railway trains on level tracks with welded rails," *Journal of Sound and Vibration*, vol. 128, no. 3, pp. 524–527, 1989.

[32] M. Schevenels, "The impact of uncertain dynamic soil characteristics on the prediction of ground vibrations," 2007.